38th International Electric Vehicle Symposium and Exhibition (EVS38)
Göteborg, Sweden, June 15-18, 2025

Adaptive Extended Kalman Filter-Based State of Charge Estimation for a Lithium-Ion Battery Module

Qian Xun[1], Gustavo Gomez Casanova[1,2], Xiaoliang Huang[1]
[1]*Qian Xun (corresponding author) RISE Research Institutes of Sweden, Borås, Sweden, qian.xun@ri.se*
[2]*University of L'Aquila, L'Aquila, Italy*

Executive Summary

As battery electric vehicles continue to drive the shift toward sustainable transportation, accurate and robust state of charge (SoC) estimation for lithium-ion batteries become essential for reliable battery management. This paper presents an adaptive extended Kalman filter (AEKF)-based framework for SoC estimation, utilizing a second-order equivalent circuit model. Model parameters are identified through nonlinear optimization using reference performance test data, with the setting of time constant constraints guided by preliminary exponential fitting. To improve the accuracy of the SoC estimation, the initial error covariance matrix, process noise covariance, and measurement noise covariance are jointly optimized using a genetic algorithm, aiming to minimize the root mean square error between the estimated SoC and the Coulomb counting based calculation. The AEKF adaptively adjusts the process noise covariance in real-time based on estimation residuals, thereby improving robustness. Comparative simulations under both ideal and perturbed scenarios, including initial SoC deviation, sensor noise, and parameter mismatch, demonstrate that the proposed AEKF significantly outperforms the conventional EKF method.
Keywords: Electric vehicles, batteries, battery management systems, energy storage systems.

1 Introduction

The global transition towards sustainable transportation has significantly accelerated the adoption of battery electric vehicles (BEVs) [1]. By 2023, the number of electric cars registered worldwide surpassed 40 million, fueled by advancements in battery technologies, declining costs, and favorable government policies [2]. Lithium-ion batteries (LIBs) remain the dominant energy storage technology in BEVs due to their relatively high energy and power density, long lifespan, and relatively low self-discharge rates.

Effective battery management systems (BMS) are essential to ensure the reliability, safety, and performance of LIBs. A critical function of the BMS is the accurate and robust estimation of the state of charge (SoC), which directly influences range prediction, charge scheduling, and battery health management [3]. However, SoC estimation remains challenging due to the inherently nonlinear electrochemical dynamics of LIB, the inaccessibility of internal states, and the time-varying nature of battery parameters under real-world conditions [4].

Various techniques have been developed for SoC estimation in LIB, including Coulomb counting (CC), open-circuit voltage (OCV) look-up tables, equivalent circuit models (ECMs), electrochemical models, and data-driven approaches [5, 6]. Among these, ECM-based model-driven methods offer a favorable balance between model accuracy and implementation complexity, making them particularly attractive for BMS deployment in EVs. Within this framework, SoC is estimated as an internal state variable based on the real-time input and output measurements (i.e., current and voltage), using filtering techniques.

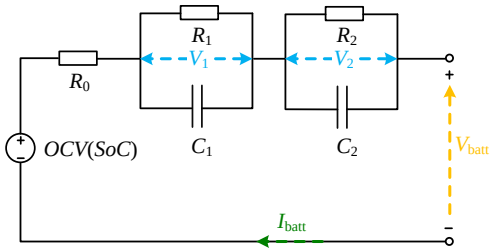

Figure 1: Equivalent circuit model with 2RC branches.

Among these, model-based filtering techniques based on ECMs strike a favorable balance between accuracy and computational efficiency, making them well suited for onboard SoC estimation [7]. This has motivated widespread adoption of Kalman filter (KF)-based approaches.

The KF and its derivatives have gained widespread adoption in this context due to their recursive nature and capability to handle noisy measurements and model uncertainties. In particular, the extended Kalman filter (EKF) enables online estimation in nonlinear systems by linearizing the battery model around the current state estimate, accommodating the nonlinear OCV–SoC relationship in practical applications [8]. The EKF has been widely used with ECMs, especially the first-order and second-order resistance-capacitance (RC) networks, to provide real-time SoC estimation under varying load profiles.

However, the performance of the EKF is strongly influenced by the appropriate selection of the process noise covariance ($\boldsymbol{Q}$) and measurement noise covariance ($\boldsymbol{R}$) matrices. These matrices govern the filter confidence in model prediction versus measurement correction. In practice, fixed $\boldsymbol{Q}$ and $\boldsymbol{R}$ values are often manually tuned based on limited datasets or heuristic trial-and-error. Such static tuning leads to suboptimal estimation accuracy, particularly when the system undergoes time-varying conditions, such as temperature changes, load transients, or cell degradation. In these cases, the mismatch between assumed and actual noise statistics can result in significant estimation errors or filter divergence.

To address these limitations, adaptive extended Kalman filter (AEKF) methods have been introduced, where the noise covariances are dynamically adjusted based on real-time innovation statistics (i.e., the residual between predicted and measured voltages). By updating $\boldsymbol{Q}$ adaptively in response to the observed behavior of the system, the AEKF improves robustness and tracking performance under a broader range of operating conditions. Several adaptation strategies have been explored in the literature, such as covariance matching, forgetting factor approaches, and residual-based scaling [6, 9]. These methods seek to strike a balance between responsiveness to new information and stability of the filter update.

In this paper, a robust AEKF-based SoC estimation method is proposed for LIB modules. The core contributions are as follows:

- A 2RC equivalent circuit model is employed, with parameters identified via constrained nonlinear optimization using reference performance test (RPT) data.
- A 9th-degree polynomial is adopted to capture the nonlinear OCV–SoC behavior, supporting accurate local linearization for EKF-based SoC estimation.
- A genetic algorithm is used to jointly optimize the initial values of matrices $\boldsymbol{P}$, $\boldsymbol{Q}$, and $\boldsymbol{R}$ to minimize SoC estimation error.
- An AEKF is implemented to enhance the accuracy and robustness of the SoC estimation under initial SoC bias, current noise, and model mismatch compared to conventional EKF.

The remainder of this paper is organized as follows: Section 2 describes the battery modeling and parameter identification. Section 3 presents the development of the AEKF-based SoC estimation framework. Section 4 discusses the simulation setup and results. Finally, Section 5 concludes the paper and outlines directions for future work.

2 Battery Modeling and Parameter Identification

Accurate battery modeling is fundamental for effective state estimation in BMS. In this work, a second-order ECM, commonly referred to as the 2RC model, is employed to characterize the dynamic behavior of the LIB module. This model provides a balance between model accuracy and computational simplicity, making it well-suited for real-time SoC estimation.

2.1 Battery Equivalent Circuit Model

The 2RC ECM consists of an open-circuit voltage (OCV) source in series with an ohmic resistance R_0, and two parallel RC branches with $R_1 - C_1$ and $R_2 - C_2$ representing the battery polarization dynamics. The schematic of the model is shown in Fig. 1.

The terminal voltage $V_{\text{batt}}(k)$ at discrete time k is given by

$$V_{\text{batt}}(k) = OCV(SoC(k)) - R_0 \cdot I(k) - V_1(k) - V_2(k) \tag{1}$$

where $OCV(SoC(k))$ is the open-circuit voltage as a function of the SoC, $SoC(k)$ is the SoC at time step k, $I(k)$ is the current where positive for discharging and negative for charging, $V_1(k)$ and $V_2(k)$ are the voltages across the first and second RC branches, respectively.

The dynamics of the RC branch voltages are governed by

$$V_1(k) = V_1(k-1) \cdot \exp\left(-\frac{\Delta t}{R_1 C_1}\right) + \left(1 - \exp\left(-\frac{\Delta t}{R_1 C_1}\right)\right) \cdot I(k-1) \cdot R_1 \tag{2}$$

$$V_2(k) = V_2(k-1) \cdot \exp\left(-\frac{\Delta t}{R_2 C_2}\right) + \left(1 - \exp\left(-\frac{\Delta t}{R_2 C_2}\right)\right) \cdot I(k-1) \cdot R_2 \tag{3}$$

where Δt is the sampling time interval.

2.2 Parameter Identification Methodology

The parameters R_0, R_1, R_2, C_1, and C_2 encapsulate the battery internal resistance and dynamic polarization characteristics. Proper identification of these parameters is critical to ensure accurate battery voltage prediction and, consequently, reliable SoC estimation. The parameter identification is performed using a nonlinear optimization approach. Experimental data from a RPT, which includes dynamic current pulses and the corresponding terminal voltage response, is utilized for this purpose.

The objective function of the optimization is defined as the minimization of the root mean squared errors (RMSE) between the measured terminal voltage $V_{\text{meas}}(k)$ and the model-predicted terminal voltage $V_{\text{model}}(k)$ over all time steps N, and the RMSE can be written as

$$\text{RMSE}_{\text{V}}(\boldsymbol{\theta}_1) = \sqrt{\frac{1}{N}\sum_{k=1}^{N}\left(V_{\text{meas}}(k) - V_{\text{model}}(k;\boldsymbol{\theta}_1)\right)^2} \tag{4}$$

The optimization problem is formulated as

$$\min_{\boldsymbol{\theta}_1} \quad \text{RMSE}_{\text{V}}(\boldsymbol{\theta}_1) \tag{5a}$$

$$\text{subject to} \quad \boldsymbol{\theta}_{1\text{lb}} \leq \boldsymbol{\theta}_1 \leq \boldsymbol{\theta}_{1\text{ub}} \tag{5b}$$

$$c_i(\boldsymbol{\theta}_1) \leq 0, \quad i = 1, \ldots, m \tag{5c}$$

where $\boldsymbol{\theta}_1 = [R_0, R_1, R_2, C_1, C_2]$ represents the parameter vector. Constraint (5b) imposes simple bound constraints to ensure physically meaningful parameter values, while constraint (5c) includes nonlinear inequalities that enforce the following:

- The time constants of both RC branches lie within realistic ranges;
- A clear time-scale separation between the fast and slow branches is maintained, i.e., $R_1 C_1 \ll R_2 C_2$;
- A structural condition such as $R_2 < 0.5 R_1$ is satisfied.

3 Kalman Filter-Based SoC Estimation

Accurate SoC estimation for LIB requires a robust observer capable of handling system nonlinearities and uncertainties. In this work, an AEKF is developed to enhance the SoC estimation performance by dynamically adjusting the process noise covariance based on real-time innovation statistics.

3.1 State-Space Model Formulation

The battery model described in Section 2 can be reformulated into a discrete-time state-space representation suitable for KF. The state vector is defined as

$$\boldsymbol{x}(k) = \begin{bmatrix} SoC(k) \\ V_1(k) \\ V_2(k) \end{bmatrix}$$

The system dynamics are given by

$$\boldsymbol{x}(k+1) = \boldsymbol{A}\boldsymbol{x}(k) + \boldsymbol{B}u(k) + \boldsymbol{w}(k) \tag{6}$$

$$z(k) = \boldsymbol{C}\boldsymbol{x}(k) + Du(k) + v(k) \tag{7}$$

where $u(k)$ is the input current, $z(k)$ is the measured terminal voltage, $\boldsymbol{w}(k)$ and $v(k)$ are the process and measurement noise, respectively.

The system matrices are defined as

$$\boldsymbol{A} = \begin{bmatrix} 1 & 0 & 0 \\ 0 & \exp\left(-\frac{\Delta t}{R_1 C_1}\right) & 0 \\ 0 & 0 & \exp\left(-\frac{\Delta t}{R_2 C_2}\right) \end{bmatrix}$$

$$\boldsymbol{B} = \begin{bmatrix} -\frac{\eta \Delta t}{Q_\mathrm{n}} \\ R_1\left(1 - \exp\left(-\frac{\Delta t}{R_1 C_1}\right)\right) \\ R_2\left(1 - \exp\left(-\frac{\Delta t}{R_2 C_2}\right)\right) \end{bmatrix}$$

$$\boldsymbol{C} = \begin{bmatrix} \frac{dOCV}{dSoC} & -1 & -1 \end{bmatrix}$$

$$D = -R_0$$

Here, η is the Coulombic efficiency, and Q_n is the nominal battery capacity.

3.2 Extended Kalman Filter Equations

The nonlinear measurement function, mainly due to the OCV-SoC relationship, necessitates the use of an EKF. The EKF prediction and update steps are as follows. First, the prediction step for the states and the error covariance ahead is written as

$$\hat{\boldsymbol{x}}(k+1|k) = \boldsymbol{A}\hat{\boldsymbol{x}}(k|k) + \boldsymbol{B}u(k) \tag{8}$$

$$\boldsymbol{P}(k+1|k) = \boldsymbol{A}\boldsymbol{P}(k|k)\boldsymbol{A}^T + \boldsymbol{Q}(k) \tag{9}$$

Then, the update step for the Kalman gain, the state estimation with the measurement z_k, and the error covariance is written as

$$\boldsymbol{K}(k+1) = \boldsymbol{P}(k+1|k)\boldsymbol{C}^T \left(\boldsymbol{C}\boldsymbol{P}(k+1|k)\boldsymbol{C}^T + R(k)\right)^{-1} \tag{10}$$

$$\hat{\boldsymbol{x}}(k+1|k+1) = \hat{\boldsymbol{x}}(k+1|k) + \boldsymbol{K}(k+1)\left(z(k+1) - \boldsymbol{C}\hat{\boldsymbol{x}}(k+1|k) - Du(k+1)\right) \tag{11}$$

$$\boldsymbol{P}(k+1|k+1) = \left(\boldsymbol{I} - \boldsymbol{K}(k+1)\boldsymbol{C}\right)\boldsymbol{P}(k+1|k) \tag{12}$$

where $\boldsymbol{I}$ is the identity matrix.

3.3 OCV-SOC Polynomial Approximation

The OCV-SoC relationship is inherently nonlinear. To integrate it into the EKF framework, the curve is approximated using a 9th-degree polynomial fit, expressed as

$$OCV(SoC) \approx a_0 + a_1 SoC + a_2 SoC^2 + \cdots + a_9 SoC^9 \tag{13}$$

The derivative $\frac{dOCV}{dSoC}$ required for the matrix $\boldsymbol{C}$ is analytically computed by differentiating the fitted polynomial, shown as

$$\frac{dOCV}{dSoC} = a_1 + 2a_2 SoC + 3a_3 SoC^2 + \cdots + 9a_9 SoC^8 \tag{14}$$

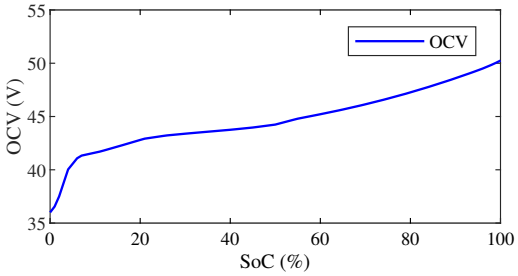

(a) OCV–SoC curve.

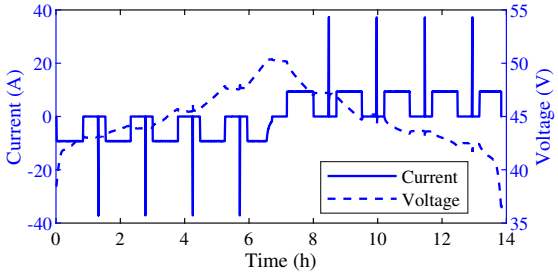

(b) Current (left) and voltage (right) vs time.

Figure 2: Experimental dataset: OCV–SoC relationship and dynamic profile of current and voltage.

3.4 Adaptive Extended Kalman Filter

To further improve estimation accuracy and robustness under varying conditions, an adaptive mechanism is implemented. The process noise covariance matrix $\boldsymbol{Q}(k)$ is updated online based on the innovation (measurement residual) at each time step

$$\boldsymbol{r}(k) = z(k) - \boldsymbol{C}\hat{\boldsymbol{x}}(k|k-1) - Du(k) \tag{15}$$

The adaptive update of $\boldsymbol{Q}(k)$ follows the following equation

$$\boldsymbol{Q}(k) = \boldsymbol{K}(k)\boldsymbol{r}(k)\boldsymbol{r}(k)^T\boldsymbol{K}(k)^T \tag{16}$$

This adaptive strategy allows the filter to adjust to changes in the system dynamics or sensor noise characteristics, improving robustness across different operating conditions.

3.5 Initial Covariance Matrix Optimization

The initial selection of the error covariance matrices in the KF, including the state estimation error covariance $\boldsymbol{P}(0)$, the process noise covariance $\boldsymbol{Q}(0)$, and the measurement noise covariance $R(0)$, plays a critical role in determining the convergence behavior and steady-state performance of the filter. Poorly chosen values may result in slow convergence, filter inconsistency, or even divergence.

To systematically determine suitable initial values, a data-driven optimization is conducted by minimizing the RMSE between the estimated and true SoC over a validation dataset. The decision variables consist of the diagonal elements of $\boldsymbol{P}(0)$, $\boldsymbol{Q}(0)$, and $R(0)$, where

- $\boldsymbol{P}(0) \in \mathbb{R}^{n\times n}$ reflects the initial confidence in the state estimate;
- $\boldsymbol{Q}(0) \in \mathbb{R}^{n\times n}$ represents the uncertainty of process dynamics (e.g., model mismatch, noise);
- $R(0) \in \mathbb{R}$ is the variance of the voltage measurement noise.

The optimization problem is formulated as

$$\min_{\boldsymbol{\theta}_2} \quad \text{RMSE}_{\text{SoC}}(\boldsymbol{\theta}) \tag{17a}$$

$$\text{subject to} \quad \boldsymbol{\theta}_{2\text{lb}} \leq \boldsymbol{\theta}_2 \leq \boldsymbol{\theta}_{2\text{ub}} \tag{17b}$$

where $\boldsymbol{\theta}_2$ is the vector of tunable diagonal entries from $\boldsymbol{P}(0)$, $\boldsymbol{Q}(0)$, and $R(0)$. Bound constraints (17b) ensure the parameters remain within physically realistic ranges to maintain filter stability.

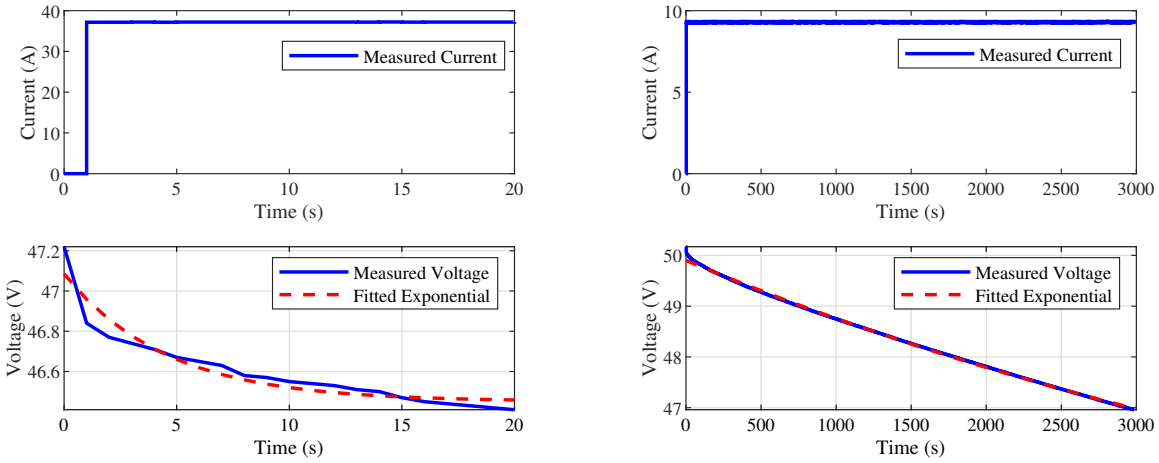

(a) Fast dynamics.

(b) Slow dynamics.

Figure 3: Exponential fitting of voltage relaxation segments for estimating characteristic time constants.

4 Simulation Results and Discussion

4.1 Dataset Description

The experimental dataset is obtained from a fresh 12S1P NMC LIB module with a nominal capacity of 37 Ah. The testing is conducted at an ambient temperature of 25°C. The test profile includes a sequence of dynamic charge and discharge pulses with current amplitudes of ±9 A to ±37 A, designed to excite the battery dynamics across a wide operating range. The voltage and current signals are sampled at a frequency of 1 Hz using high-precision measurement equipment. Fig. 2 illustrates the dataset characteristics. The OCV–SoC curve shown in Fig. 2(a) is obtained under quasi-static conditions and Fig. 2(b) shows the applied dynamic current profile and the corresponding voltage response.

4.2 Parameter Identification and Model Validation

To ensure physical interpretability and effective optimization, a preliminary analysis using single exponential fitting is conducted prior to parameter identification. This allows for an informed estimation of the dominant time constants, which guides the initialization and constraint setting for the model parameters.

4.2.1 Preliminary Exponential Fitting for Time Constant Estimation

To capture the dynamic characteristics of the battery module, two representative voltage relaxation segments are selected. Each segment is fitted using a single exponential function of the form:

$$V(t) = V_\infty + (V_0 - V_\infty) \exp\left(-\frac{t}{\tau}\right)$$

where V_∞ is the final steady-state voltage, V_0 is the initial voltage at the beginning of the relaxation, τ is the time constant.

Fig. 3 shows the fitting results, and the extracted time constants are 4.52s for fast relaxation and 5949.5s for slow relaxation. These fitted values span more than three orders of magnitude, indicating the necessity of a dual time-constant model such as the 2RC structure. They are used to guide the selection of initial values and constraint bounds for the subsequent parameter identification process.

4.2.2 Voltage Fitting Results

The MATLAB function *fmincon* is employed to solve the optimization problem formulate in (5). The accuracy of the identified 2RC equivalent circuit model is validated by comparing the model-predicted terminal voltage against the measured voltage under the dataset described in Section 4.1. Fig. 4 illustrates the comparison between the measured terminal voltage and the voltage predicted by the 2RC model

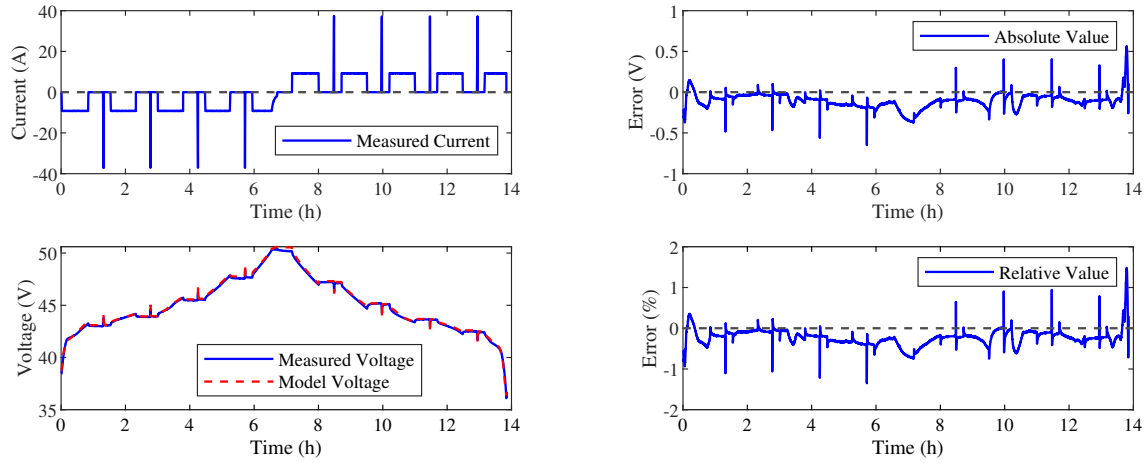

(a) Comparison of measured and model-predicted voltages.

(b) Absolute voltage error and relative voltage error.

Figure 4: Validation of the identified 2RC equivalent circuit model under dynamic current pulses.

Table 1: 2RC ECM fitted parameters

Parameter	R_0	R_1	R_2	C_1	C_2
Value	$1.30 \times 10^{-2}\Omega$	$1.64 \times 10^{-2}\Omega$	$7.23 \times 10^{-3}\Omega$	2.96×10^{2}F	7.67×10^{5}F

using the identified parameters. As shown in Fig. 4, the model-predicted voltage closely matches the experimental measurements, with a RMSE of 0.31%. The relative voltage error remains within ±1.5% throughout the test. This validates the effectiveness of the parameter identification method with proper normalization.

4.2.3 Identified Model Parameters

The final identified parameters for the 2RC model are summarized in Table 1. These parameters indicate that the battery exhibits two distinct dynamic responses: a fast dynamic response associated with the R_1C_1 branch and a slower dynamic response associated with the R_2C_2 branch. Both time constants are effectively captured by the identified model.

4.3 SoC Estimation Results

The performance of the AEKF for SoC estimation is evaluated based on the dataset described in Section 4.1. The results include the OCV-SOC curve fitting, covariance matrix optimization outcomes, the SoC estimation performance comparison, and the sensitivity analysis of SoC estimation with perturbations.

4.3.1 OCV-SOC Polynomial Fitting

The OCV–SoC relationship is modeled using a 9th-degree polynomial fitted to experimental data obtained under low-current conditions. The polynomial form and fitting method are described previously in Section 3. To evaluate the quality of the OCV–SoC polynomial fitting, the coefficient of determination R^2 is used. It quantifies how well the fitted curve explains the variance in the measured OCV data and is defined as

$$R^2 = 1 - \frac{SS_{\text{res}}}{SS_{\text{tot}}} \tag{18}$$

where SS_{res} is the residual sum of squares between the measured and fitted OCV values, and SS_{tot} is the total variance in the measured data. An R^2 value closer to 1 indicates a better fit [10].

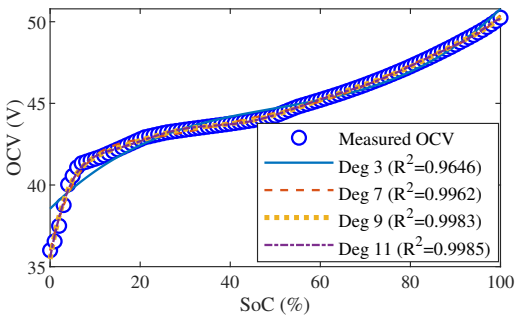

(a) Polynomial fitting of SoC–OCV curve.

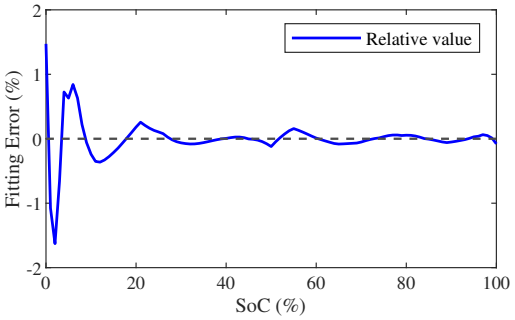

(b) Relative fitting error of the 9th-degree polynomial.

Figure 5: OCV curve fitting and error analysis.

Table 2: Optimized initial covariance matrix elements

Matrix Element	Optimized Value	Unit
$P_{11}(0)$ (SoC)	0.99	-
$P_{22}(0)$ (V_1)	0.87	V^2
$P_{33}(0)$ (V_2)	4.96	V^2
$Q_{11}(0)$ (SoC)	1.62	-
$Q_{22}(0)$ (V_1)	1.98	V^2
$Q_{33}(0)$ (V_2)	1.91	V^2
$R(0)$ (Voltage measurement noise)	0.99	V

Fig. 5 illustrates both the fitting results for multiple polynomial degrees and the residual error for the selected 9th-degree model. While higher-order polynomials yield marginally better fits, the 9th-degree polynomial achieves a desirable trade-off between accuracy and model complexity. The 9th-degree polynomial fit yields a maximum absolute error of 0.4 V and a relative error within ±2%, with best accuracy achieved in mid-SoC range and larger deviations observed at low SoC due to stronger nonlinearity.

4.3.2 Initial Covariance Matrices Optimization

The initial values of the covariance matrices, optimized using the MATLAB function *ga*, are summarized in Table 2. These optimized values are used as the initial covariance matrices for the AEKF implementation.

4.3.3 SoC Estimation Performance

To evaluate the SoC estimation accuracy under dynamic load profiles, both EKF and AEKF are implemented using the equivalent circuit parameters identified earlier. The CC method is used as a reference baseline. The initial state covariance matrix $\boldsymbol{P(0)}$ and the measurement noise covariance $R(0)$ are fixed across both filters based on the optimal values identified through AEKF. For fair comparison, the process noise covariance matrix $\boldsymbol{Q(0)}$ is optimized separately.

As shown in Fig. 6(a), the SoC estimated by AEKF closely follows the CC reference, with only minor deviations throughout the profile. In comparison, the EKF exhibits more pronounced fluctuations, particularly during sharp current transients. This discrepancy is more evident at low SoC levels, where the estimation becomes less reliable. Fig. 6(b) further confirms this trend: the relative SoC error of AEKF stays within $\pm 1\%$ across most of the profile, except in the low SoC region, where errors can exceed 10%, as indicated by the shaded gray area. In contrast, EKF errors can surpass 5% even at moderate SoC levels during rapid dynamic changes.

In addition to SoC tracking, both EKF and AEKF can reconstruct the terminal voltage in real time based on the internal RC model states and current input. Fig. 7(a) shows that both EKF and AEKF accurately follow the measured terminal voltage, with negligible deviation. The relative voltage errors plotted in

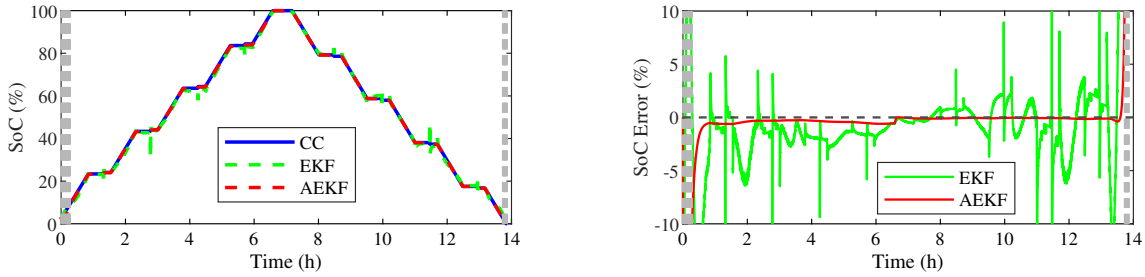

(a) SoC estimation results.

(b) Relative SoC error compared with CC.

Figure 6: Comparison of SoC estimation between EKF and AEKF under pulse load profile.

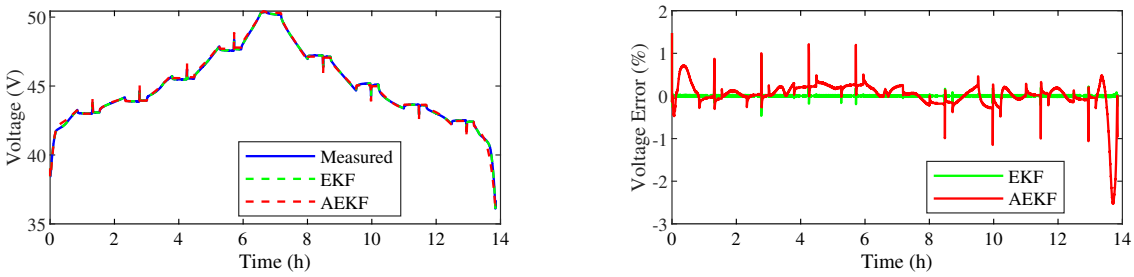

(a) Voltage estimation results.

(b) Relative voltage error compared with measurement.

Figure 7: Comparison of voltage estimation between EKF and AEKF under pulse load profile.

Fig. 7(b) remain within $\pm 2.5\%$, confirming the reliability of both algorithms in voltage estimation. Interestingly, although the SoC deviation is significant in EKF, the impact on voltage estimation is marginal due to the flatness of the OCV–SoC curve in the mid-range.

4.3.4 Sensitivity Analysis of SoC Estimation

To evaluate the robustness of the proposed AEKF under real-world uncertainties, sensitivity analysis is conducted using the same dynamic test dataset. Three types of perturbations are introduced: (i) initial SoC deviation, (ii) current measurement noise, and (iii) model parameter variation. The performance of the EKF and the AEKF is compared with the CC method used as reference.

Fig. 8 shows the results with the initial SoC setting as twice of the true value. Both EKF and AEKF gradually corrects the deviation over time. However, AEKF demonstrates superior convergence and significantly lower relative SoC error throughout the entire cycle. EKF exhibits large deviations during

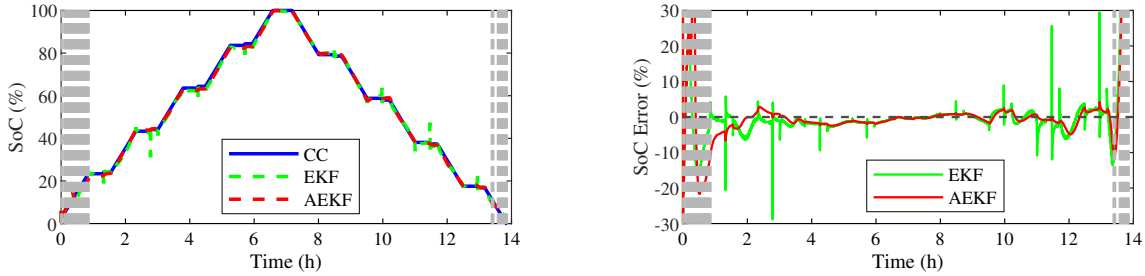

(a) Estimated SoC curves.

(b) Relative error with respect to CC method.

Figure 8: SoC estimation comparison between EKF and AEKF with initial SoC deviating twice of the true value.

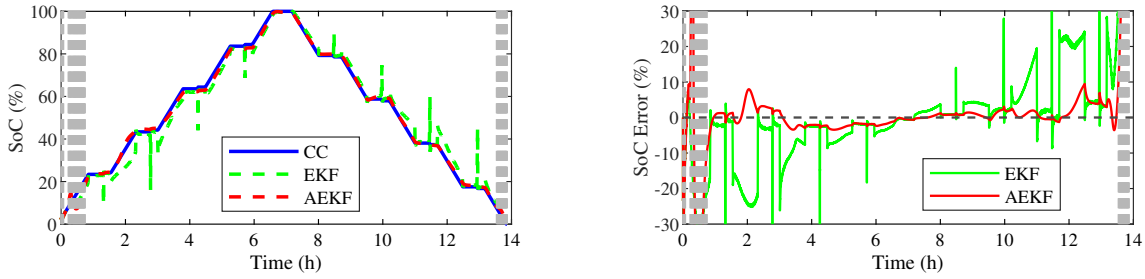

(a) Estimated SoC curves. (b) Relative error with respect to CC method.

Figure 9: SoC estimation comparison between EKF and AEKF under 0.2% current sensor noise.

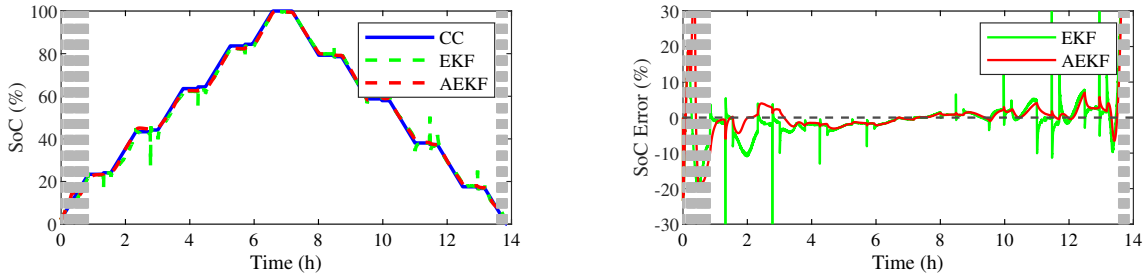

(a) Estimated SoC curves. (b) Relative error with respect to CC method.

Figure 10: SoC estimation comparison between EKF and AEKF under 20% resistance and capacitance perturbation.

mid-cycle, indicating its higher sensitivity to initialization errors.

Fig. 9 depicts the scenario where a 0.2% random noise is added to the current input. The AEKF maintains a relatively stable SoC trajectory with moderate error, while EKF fluctuates significantly, especially in segments with frequent current transitions. The adaptive update mechanism in AEKF helps suppress the noise effect more effectively.

Fig. 10 evaluates robustness when all resistances are increased by 20% and all capacitances are decreased by 20%, simulating modeling errors. AEKF again outperforms EKF by maintaining close alignment with the CC reference. The error in EKF accumulates over time due to the uncorrected model mismatch, while AEKF adaptes its process covariance to partially compensate for the discrepancy.

Overall, these results confirm that AEKF provides more robust SoC estimation performance under various real-world uncertainties compared to the conventional EKF.

5 Conclusion

This paper presents an AEKF-based method for accurate and robust SoC estimation of a LIB module. A 2RC model is employed to characterize the battery dynamics, and its parameters are identified through a nonlinear optimization approach.

To enhance the estimation performance, the initial values of the state estimation error covariance, process noise covariance, and measurement noise covariance matrices are optimized using a GA, minimizing the SoC estimation error over a validation dataset. A 9th-degree polynomial is used to approximate the nonlinear OCV–SoC curve, providing the smooth derivative needed for local linearization in EKF. Simulation results demonstrates that the proposed AEKF method significantly outperforms the conventional EKF approach, achieving a substantial reduction of RMSE in SoC estimation. The identified 2RC model also exhibits good predictive capability, with voltage fitting errors below 1.5%.

Despite these promising results, the proposed method relies on the assumption of consistent model accuracy and is validated under controlled laboratory conditions. Future work will focus on extending

the validation to aged battery modules, incorporating temperature-dependent effects into the modeling framework, and investigating lightweight adaptive filtering strategies suitable for real-time implementation under variable operating conditions. On the other hand, while the proposed AEKF offers improved estimation accuracy and robustness, its computational complexity is higher than standard EKF. Future work will explore lightweight adaptive schemes suitable for embedded BMS hardware.

Acknowledgments

The authors would like to thank Volvo Energy AB for providing the measurement data of battery module.

References

[1] B. Majmunovic, R. Sarda, R. Teodorescu, C. Lascu, and M. Ricco, "Highly efficient smart battery pack for EV drivetrains," in *2017 IEEE Vehicle Power and Propulsion Conference (VPPC)*, 2017, pp. 1–5.

[2] T. Gül and A. F. Pales, "Global ev outlook 2024 – analysis," Global EV Outlook 2024, Apr. 2024, accessed: 2024-09-13. [Online]. Available: https://www.iea.org/reports/global-ev-outlook-2024.

[3] S. Mishra, S. C. Swain, and R. K. Samantaray, "A review on battery management system and its application in electric vehicle," in *2021 International Conference on Advances in Computing and Communications (ICACC)*, 2021, pp. 1–6.

[4] Y. Wang, J. Tian, Z. Sun, L. Wang, R. Xu, M. Li, and Z. Chen, "A comprehensive review of battery modeling and state estimation approaches for advanced battery management systems," *Renewable and Sustainable Energy Reviews*, vol. 131, p. 110015, 2020.

[5] H. M. Hussein, A. Aghmadi, M. S. Abdelrahman, S. M. S. H. Rafin, and O. Mohammed, "A review of battery state of charge estimation and management systems: Models and future prospective," *WIREs Energy and Environment*, vol. 13, no. 1, 1 2024.

[6] H. He, R. Xiong, H. Guo, and S. Li, "Comparison study on the battery models used for the energy management of batteries in electric vehicles," *Energy Conversion and Management*, vol. 64, pp. 113–121, 2012.

[7] F. Yang, D. Shi, and K.-H. Lam, "Modified extended Kalman filtering algorithm for precise voltage and state-of-charge estimations of rechargeable batteries," *Journal of Energy Storage*, vol. 56, p. 105831, 2022.

[8] G. L. Plett, "Extended kalman filtering for battery management systems of LiPB-based HEV battery packs: Part 1. background," *Journal of Power Sources*, vol. 134, no. 2, pp. 252–261, 2004.

[9] H. Wei, X. Chen, Z. Lü, Z. Wang, and L. Chen, "Online estimation of lithium-ion battery state of health using grey neural network," *Power System Technology*, vol. 41, pp. 4038–4044, 2017.

[10] D. C. Montgomery, E. A. Peck, and G. G. Vining, *Introduction to Linear Regression Analysis*, 5th ed. John Wiley & Sons, 2012.

Presenter Biography

Qian Xun received her Ph.D. in Electric Power Engineering from the Chalmers University of Technology, Sweden, in 2022. She is currently a Senior Researcher at the Unit of Energy Conversion, RISE Research Institutes of Sweden, Sweden. She previously was a Research Fellow at the Center of Electronic Energy Systems, Fraunhofer Institute for Silicon Technology ISIT, Germany. Her research focuses on modeling, control, and optimization of hydrogen energy storage systems for automotive and microgrid applications, power electronics, motion control, and wide band-gap devices.